PREDICTION OF LIGHT GAS DISTRIBUTION IN CONTAINMENT EXPERIMENTAL FACILITIES USING CFX4 CODE: JOZEF STEFAN INSTITUTE EXPERIENCE

Ivo Kljenak, Miroslav Babić, Borut Mavko
Reactor Engineering Division
Jozef Stefan Institute
Jamova 39, Ljubljana, Slovenia
E-mail: ivo.kljenak@ijs.si, miroslav.babic@ijs.si, borut.mavko@ijs.si

Abstract

Two and three-dimensional simulations of experiments on atmosphere mixing and stratification in a nuclear power plant containment were performed with the code CFX4.4, with the inclusion of simple models for steam condensation. The purpose was to assess the applicability of the approach to simulate the behaviour of light gases in containments at accident conditions. The comparisons of experimental and simulated results show that, despite a tendency to simulate more intensive mixing, the proposed approach may replicate the non-homogeneous structure of the atmosphere reasonably well.

Introduction

One of the nuclear reactor safety issues that have lately been considered using Computational Fluid Dynamics (CFD) codes is the problem of predicting the eventual non-homogeneous concentration of light flammable gas (hydrogen) in the containment of a nuclear power plant (NPP) at accident conditions. During a hypothetical severe accident in a Pressurized Water Reactor NPP, hydrogen could be generated due to Zircaloy oxidation in the reactor core. Eventual high concentrations of hydrogen in some parts of the containment could cause hydrogen ignition and combustion, which could threaten the containment integrity. The purpose of theoretical investigations is to predict hydrogen behaviour at accident conditions prior to combustion.

In the past few years, many investigations about the possible application of CFD codes for this purpose have been started [1-5]. CFD codes solve the transport mass, momentum and energy equations when a fluid system is modelled using local instantaneous description. Some codes, which also use local instantaneous description, have been developed specifically for nuclear applications [6-8]. Although many CFD codes are multi-purpose, some of them still lack some models, which are necessary for adequate simulations of containment phenomena. In particular, the modelling of steam condensation often has to be incorporated in the codes by the users.

These theoretical investigations are complemented by adequate experiments. Recently, the following novel integral experimental facilities have been set up in Europe: TOSQAN [9,10], at the Institut de Radioprotection et de Sureté Nucléaire (IRSN) in Saclay (France), MISTRA [9,11], at the

Commissariat à l' Energie Atomique (CEA) in Saclay (France) and ThAI [12,13] at Becker Technologies GmbH in Eschborn (Germany). A multi-compartment experimental facility has also been set up in South Korea [14]. Most of these novel facilities are equipped with instrumentation that allows measurement of local temperature, species concentration and velocities. Thus, the non-homogeneous structure and the flow patterns in the containment atmosphere may be observed, which enables a better understanding of mixing and stratification processes relevant for the response of the containment of an actual nuclear power plant. Besides, local experimental measurements may be used to assess the validity of simulations performed by CFD codes.

At the Jozef Stefan Institute (JSI), experiments performed in the TOSQAN and ThAI experimental facilities were simulated with the CFD code CFX4.4 [15] within the participation in the OECD International Standard Problem No. 47 (ISP-47) [9,13,16,17]. The simulations were performed with the knowledge of experimental results. The CFX code has already been used by other authors for similar simulations [18]. Also, analyses of similar experiments have also been carried out by other authors [19,20]. In particular, both experiments have been simulated by other participants in the ISP-47 [16,17]. In the present work, an overview and synthesis of the simulations performed at JSI [21-25] is provided.

Computational modelling

The CFX4.4 code [15] is a general purpose CFD code, which has been first developed by AEA Technology (UK) and is now being developed by ANSYS Inc. The code solves the conservation equations for mass, momentum and energy together with their initial and boundary conditions. The discretisation of the equations in the CFX code is based on a conservative finite-volume method. A non-staggered grid arrangement is employed, where all the variables (velocity components and scalars) are stored in the geometrical centres of control volumes (cells) that fill up the considered flow domain.

Generic features of CFX models for TOSQAN and ThAI facilities

The atmosphere in the facilities was modelled as single-phase. The air-steam, air-steam-helium and air-steam-helium-fog atmospheres were treated as single-phase gaseous mixtures that are homogeneous within each computational cell, with air as the "carrier fluid" [15]. The following options were prescribed in the CFX models:

— compressible flow,
— turbulent flow (k-ε model),
— buoyant flow,
— no-slip condition at the vessel wall.

The convective heat transfer between the vessel atmosphere and the heat structures was calculated by the CFX code.

Wall condensation model

One of the features, which are not yet commonly included in CFD codes and has to be implemented by the user, is the modelling of steam condensation. Two main approaches have been proposed by various authors to model wall condensation in CFD codes. One approach [1,26,27] is modelling based on first principles: heat and mass transfer on condensation surfaces are modelled

using basic physical laws. Although this approach will probably prevail in the future, its main drawback at present is that a very fine computational grid is necessary near the condensation surface, which causes long computation times.

Another approach [3,4,5,28] is to include heat or mass transfer correlations that were originally developed for "integral" (volume-averaged) calculations and apply them in the layer of cells contiguous to the condensation surface. In these correlations, some physical variables pertaining to the "bulk flow" usually appear. One of the problems is the choice of appropriate values of the "bulk flow" parameters from the computational grid used by the CFD code. If values from the cells contiguous to the condensation surface are applied, then relatively large cells must be used, which may not be adequate for modelling other near-wall phenomena. Besides, as CFD codes were developed to solve equations that are derived from first principles, using local instantaneous description, the inclusions of correlations, which are based on averaged physical quantities and provide average condensation rates, is somehow contrary to the basic "philosophy" of CFD. However, this approach allows relatively fast calculations and may prove adequate for industrial applications.

In the present work, the second approach was used. Steam condensation was modelled as a sink of mass and enthalpy by applying the correlation by Uchida et al. [29] that was basically developed for an integral approach. The condensate film on "cold" structures was not considered. The Uchida correlation is based on experiments on forced convection. Basically, the steam condensation rate is obtained from the expression:

$$m^0 = C_u \, (\rho_{steam}/\rho_{nc})^{0.8} \cdot A \cdot (T - T_{wall}) \, / \, h_{lg} \qquad (1)$$

where C_u is an adjustable coefficient, h_{lg} denotes the latent heat of evaporation, ρ_{steam} and ρ_{nc} the densities of steam and non-condensable gases, T the gas temperature, T_{wall} the wall temperature and A the area of the cell face at the condensation surface. All the physical variables, except T_{wall}, refer to "bulk flow" conditions in the vessel.

As the correlation depends only on the temperature difference between gas and wall, condensation may be simulated even if the steam density is lower than the saturation density at the condensing wall temperature. To prevent this non-physical behaviour, a limiting condition was set: the steam partial pressure must be higher than the saturation pressure at the temperature of the wall for condensation to occur. Thus, during each time step, the amount of condensed steam is limited so that the steam partial pressure never drops below the saturation pressure. The corresponding enthalpy sink H^0 (enthalpy flow) due to condensation is calculated as:

$$H^0 = m^0 \bullet (c_{p,steam} T_{cell} - c_{p,air} T_{ref}) \qquad (2)$$

where T_{ref} denotes some (fixed) reference temperature and c_p denotes the fluid specific heat at constant pressure. The reference specific enthalpy is calculated in the CFX code as the product of the specific heat of the "carrier fluid" (air in the present model) and of the reference temperature.

The modelling of condensation was implemented in a user-defined subroutine, which was included in the CFX computational tool. Sinks of mass and enthalpy occurred in cells contiguous to the condensing wall. In each cell, the mass sink was calculated from eq. (1) where the "bulk flow" physical quantities (temperature, steam density, non-condensable gas density) were evaluated at the cell centre. As the temperature of the gaseous mixture corresponding to the cell centre appears in eqs. (1) and (2), the calculated condensation rate and enthalpy sink necessarily depend on the width of cells

contiguous to the condensation surface. The value of the coefficient C_u was adjusted to obtain a good agreement between measured and calculated pressure and average atmosphere temperature in the vessel. As the cell width influences T_{cell}, C_u necessarily depends on the cell width.

Homogeneous condensation / evaporation and rain-out models

A simple mechanistic homogeneous condensation and evaporation model was also incorporated into the code. Fog was treated as a gas, but its effects on compressibility parameters were neglected. When the steam pressure P_{steam} in a cell was higher than the steam saturation pressure at the cell gas temperature P_{sat}, the homogeneous condensation rate (*i.e.* fog creation rate) was calculated from the expression:

$$m^0_B = (P_{steam} - P_{sat})V_{cell} / (R_{steam}T_{gas}) / \Delta t_1 \quad (3)$$

where Δt_1 is an adjustable relaxation parameter, with a constant value of 10 *s*. If fog was present in a cell and the steam pressure P_{steam} was lower than the steam saturation pressure P_{sat} at the cell gas temperature, the homogeneous evaporation rate was calculated from the expression:

$$m^0_E = (P_{steam} - P_{sat})V_{cell} / (R_{steam}T_{gas}) / \Delta t_1 \, . \quad (4)$$

The corresponding enthalpy source (sink) due to the release (consumption) of latent heat was determined from the expressions (for condensation and evaporation):

$$H^0_B = m^0_B \bullet h_{lg}(T_{gas}), \quad (5)$$

$$H^0_E = m^0_E \bullet h_{lg}(T_{gas}). \quad (6)$$

If the fog density was higher than 30 g/m^3, fog was removed from a cell at a rate:

$$m^0_R = (m_{fog} - 0.03\ kg/m^3\ V_{cell}) / \Delta t_{step} \bullet \Delta t_2 \quad (7)$$

with a corresponding enthalpy sink of

$$H^0 = m^0_R \bullet (c_{p,fog}T_{cell} - c_{p,air}T_{ref}) \quad (8)$$

where Δt_2 is also an adjustable relaxation parameter, with a constant value of 100 *s*. The value 30 g/m^3 is within the range of values, measured during the experiment in the ThAI vessel [17].

Simulation of TOSQAN experiment

TOSQAN experimental facility and experiment

The TOSQAN facility is a cylindrical vessel with an internal volume of 7.0 m^3 (Figure 1). The total height of the facility is 4.80 *m*, and the diameter of the main cylindrical part is 1.50 *m*. Steam and

other gases are injected through a vertical tube located at the vessel centre-line. The injection opening is located at the elevation 2.10 *m* (all elevations refer to the sump floor). The temperature of the vessel walls may be controlled, so that the walls are divided into a "hot" zone and a "cold" zone. Steam may condense on walls located in the cold zone (between elevations 2.39 *m* and 4.39 *m*), where the controlled temperature is maintained at low levels [9,10].

In the simulated test [9,10], the vessel was initially filled with air. Air, steam and helium (which was used instead of hydrogen for safety reasons) were injected intermittently with various mass flow rates. Steam condensation occurred only on walls with lower temperature. The sump, where the liquid from the condensate film collected, was drained continuously. The thermal-hydraulic behaviour was determined by the following dominant physical phenomena: gas injection, steam condensation, heat transfer and buoyant flow. A schematic view of the time-dependent injection mass flow rates and pressure in the test vessel during the experiment is shown on Figure 2. During certain phases, steady states were reached when the steam condensation rate became equal to the steam injection rate, while all boundary conditions were kept constant. The uncertainties of temperature and volumetric concentration measurements were ±1 ºC and up to ± 2.3% of the measured value, respectively [10].

TOSQAN vessel

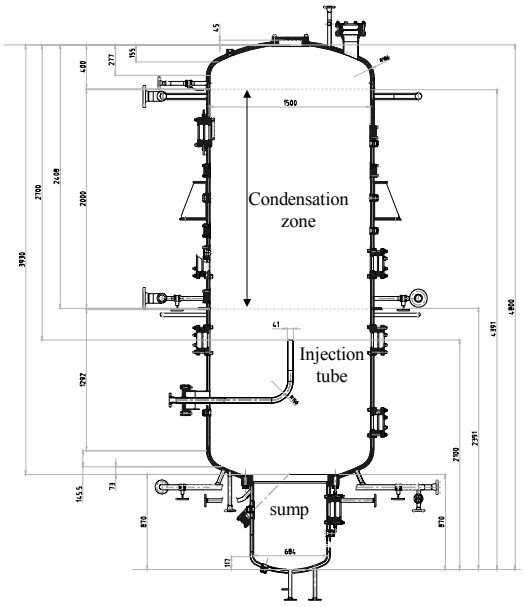

Figure 1. TOSQAN experimental facility [9].

Specific features of TOSQAN input model

A two-dimensional (2D) axisymmetric model (in cylindrical coordinates) for the code CFX4.4 was developed. Only the wall condensation model was included in the CFX code. The computational domain is a block with 160 cells in the axial (vertical) direction and 30 cells in the radial (horizontal) direction, so that there are 4800 cells altogether. The width (radial direction) of each cell depends on the axial location. Thus, cells located within the vessel sump are narrower than cells located within the main part. In the condensation zone, which includes 67 rows of cells, the width of the cells contiguous to the vessel wall is 4.0 *cm* [23]. The numerical convergence criterion was set to $0.8 \cdot 10^{-3}$ *kg/s*.

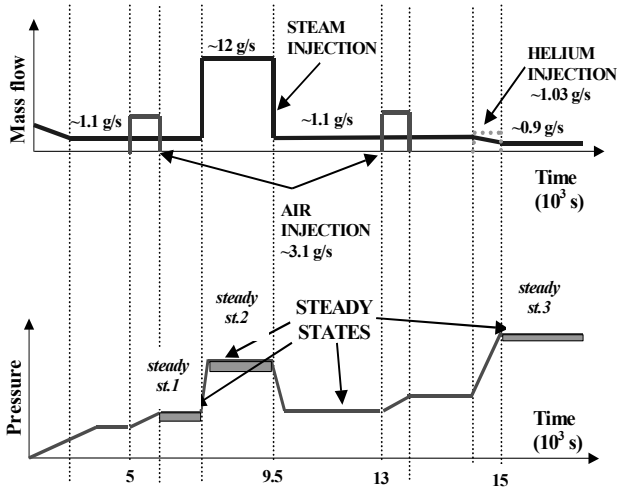

Figure 2. Schematic view of time-dependent injection mass flow rate and pressure in the TOSQAN vessel during the experiment.

Results of TOSQAN simulation

The main purpose of the TOSQAN simulations was to reproduce the non-homogeneous atmosphere during steady states 1, 2 and 3 (see Figure 2), given that the steam condensation rate is calculated adequately. The value of the coefficient C_u (eq. 1) was adjusted to obtain a good agreement between measured and calculated pressure and volume-averaged atmosphere temperature in the vessel during steady states. The same value $C_u = 354$ W/m^{2}K was used for all three steady states, which were simulated separately. The fluid was assumed to be initially at rest. For each simulation, the initial pressure and average temperature in the vessel were set to the measured values. The simulations were run until the condensation rate became equal to the steam injection mass flow rate and the variations of pressure and average temperature became small enough. The time step during the simulation varied between 0.1 and 0.25 *s*.

In the simulation of steady states 1 and 3 (during the latter, helium was present), the condensation rate calculated with the prescribed value of C_u was too high and was instead determined by the limiting condition, that the partial steam pressure cannot decrease below saturation pressure at the temperature of the wall. The condensation rate was actually determined by the value of the coefficient C_u only in the calculation of the condensation rate during steady state 2, where the steam injection and condensation rates were an order of magnitude higher.

Figures 3 to 6 show the comparison of some experimental and simulation results during steady state 3. Although the computational domain was only one half of a vertical plane, symmetric radial profiles are shown over the entire vessel for comparison with experimental data on both sides of the vessel axis. A good agreement between measured and calculated temperatures may be observed (radial profiles on Figure 3, vertical profiles on Figure 4). For the species concentration profiles (Figures 5 and 6), the simulation replicated the relatively homogeneous atmosphere (the apparently large discrepancies and irregularity of experimental results are due to the scale on the ordinata axis).

Calculations were also performed with a refined grid of 19200 cells (320 cells in the vertical direction and 60 cells in the horizontal direction), except for the width of cells contiguous to the condensation surface. The results did not show any significant difference.

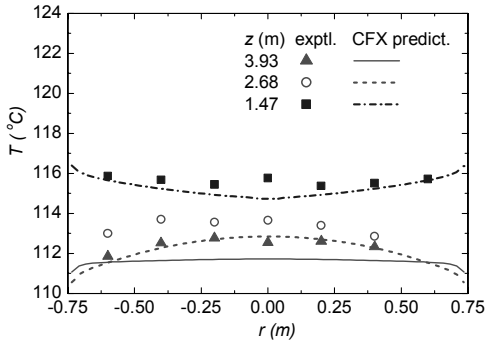

Figure 3. TOSQAN Steady state 3: experimental and simulated temperature *radial* profiles.

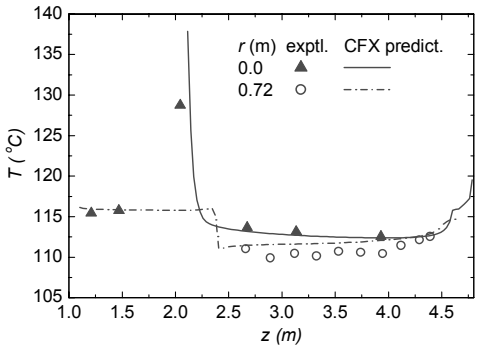

Figure 4. TOSQAN Steady state 3: experimental and simulated temperature *vertical* profiles.

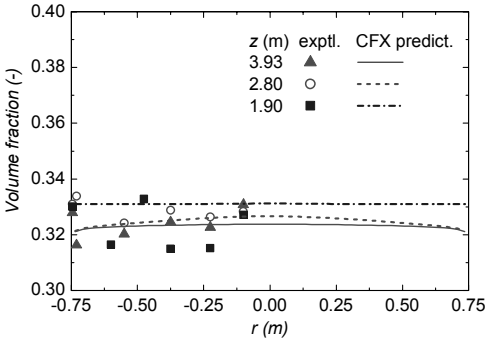

Figure 5. TOSQAN Steady state 3: experimental and simulated *radial* profiles of steam volume fraction.

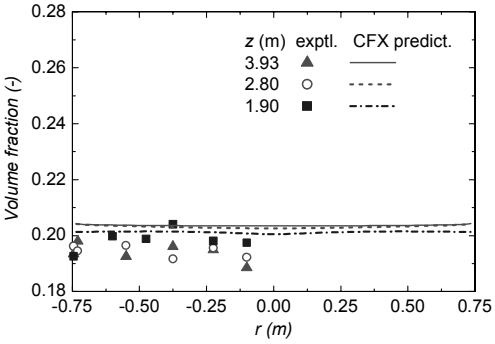

Figure 6. TOSQAN Steady state 3: experimental and simulated *radial* profiles of helium volume fraction.

Influence of cell width contiguous to the condensation surface

Simulations were also performed with the width of cells contiguous to the condensation surface set to 3.0 *cm* and 2.0 *cm*. As an illustration, Figures 7 and 8 show the calculated radial profiles of temperature and steam volume fraction for steady state 2, obtained with the cell width 4.0 *cm* ("basic" calculation) and 2.0 *cm*. Steady state 2 was selected, as the condensation rate was determined by the value of the coefficient C_u in eq. (1). There are no qualitative differences, and the quantitative differences are of the order of the uncertainties of experimental measurements. To obtain a good agreement between measured and simulated pressure, the coefficient C_u had of course to be slightly modified (see Table 1) as the use of narrower cells caused a lower value of T_b in eq. (1). The small differences between values of C_u show that the model is stable (no "cliff edge" effect). Besides, the values vary approximately linearly width the cell width, which may be considered as a first basis for establishing guidelines for modelling wall steam condensation with the proposed approach.

Cell width (m)	0.04	0.03	0.02
C_u	354.0	365.0	381.0

Table 1. Values of coefficient C_u for different widths of cells contiguous to condensation surface in TOSQAN simulations.

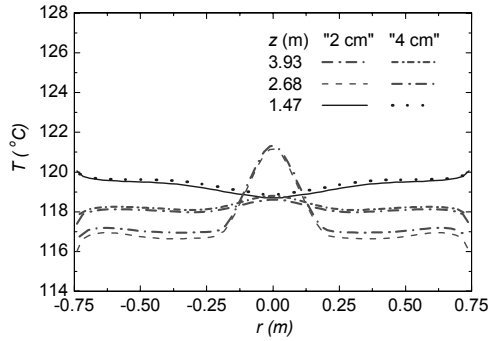

Figure 7. Radial profiles of temperature (TOSQAN steady state 2) calculated with different cell widths contiguous to the condensation surface.

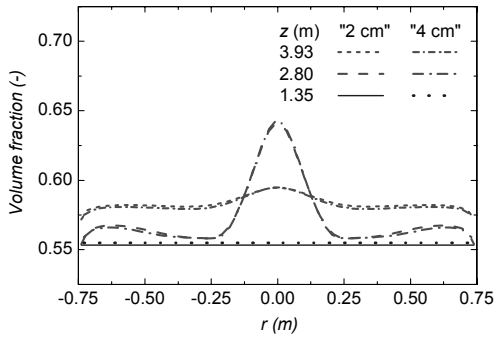

Figure 8. Radial profiles of steam volume fraction (TOSQAN steady state 2) calculated with different cell widths contiguous to the condensation surface.

Simulation of ThAI experiment

ThAI experimental facility and experiment

The main component of the ThAI facility is a cylindrical steel vessel of 9.2 *m* total height (including the sump compartment at the lower end) and 3.2 *m* diameter, with a total volume of 60 m^3 (Figure 9). The vessel space is subdivided by an open inner cylinder between elevations 2.16 *m* and 6.25 *m* relative to the sump floor, with an internal diameter of 1.38 *m* and a horizontal separation plane in the annular region with vent openings. The separation plane is located at elevation 4.00 *m* from the vessel bottom and consists of 4 equally spaced condensate-collecting trays that span from the inner cylinder wall to the vessel wall. Each tray covers 60° of the circumference. Vessel walls and internal structures are all made of steel of thickness between 15 and 130 *mm*. The outer edge of the vessel is thermally insulated by a 12 *cm* layer of rock wool and covered by 1 *mm* thick aluminium.

Initially, only air with about 70 % humidity was present in the vessel. The experiment was divided into 4 phases. During the first 2 phases, helium and steam were injected upwards in the upper part of the vessel. During the 1st phase (0-2700 s), helium was injected together with a small amount of steam. During the 2nd phase (2700-4700 *s*), steam was injected. During the 3rd phase (4700-5700 s), steam was injected in the lower part of the vessel in the horizontal direction. The last phase lasted from 5700 to 7700 *s* without any gas injection.

Specific features of ThAI input model

A three-dimensional (3D) grid was developed, covering only one half of the vessel. This was possible due to the assumption of symmetry relative to the vertical plane crossing the injection locations. The numerical grid consists of 44 cells in the vertical direction, 22 cells in the radial direction and 17 cells in the azimuthal direction. Both the wall condensation and homogeneous condensation models were included in the CFX code. Cells contiguous to the wall were 2 *cm* wide and the value of 360 W/m^2K was used for the coefficient C_u in eq. (1). This value, which is very close to the value used in the simulation of the TOSQAN experiment, was obtained by fitting experimental and calculated pressure and average atmosphere temperature for another test (TH1) that was performed in the ThAI facility as well [13]. These time-dependent values were supplied to the ISP-47 participants to help in the adjustment of their models.

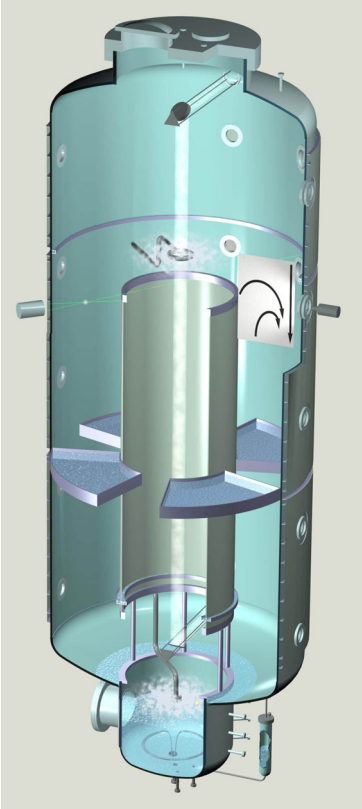

Figure 9. ThAI experimental facility [13].

Results of ThAI simulation

The main purpose of the simulation was to reproduce the non-homogeneous temperature and species concentration fields. In order to reduce the simulation time, the convergence criterion was increased from $0.5 \cdot 10^{-3}$ to $0.5 \cdot 10^{-2}$ *kg/s*, which resulted in changes of the air mass in the vessel of approximately 5 % during the entire simulation. The time step varied between 0.05 *s* and 0.2 *s*.

The positions of measurement transducers, from which time-dependent experimental data are compared to simulation results, are presented in Table 2. The vertical elevation refers to the sump floor.

Figures 10 to 13 show time-dependent variables in different parts of the vessel (the vertical lines on the figures delimit the phases of the experiment). The calculated pressure (Figure 10) agrees reasonably well with the measurements during the first three phases. This could be expected, as the value of C_u in eq. (1) was set by fitting the results of another test performed in the same facility.

However, as both condensation models are active, the agreement may not be considered as a satisfactory validation of the homogeneous condensation model. The simulated temperatures (Figure 11) during the first two phases show similar behaviour as was observed during experiment, except that the calculated temperature in the upper annulus is too high. In the 3rd phase, calculated temperatures in the vessel upper part show different behaviours than in the experiment, while in the last phase they follow the experimental trend. The agreement between experimental and simulated steam volume fractions (Figure 12) is good during the 1st and 4th phase (as the atmosphere became relatively well-

Variable	Vertical elevation *m*	Radius (dist. from axis) *m*	Azimuthal position °
Pressure	7.7	1.57	300
Temperature upper plenum	7.7	0.7	90
Temperature upper annulus	4.9	1.14	300
Temperature lower annulus	2.8	1.14	300
Temperature lower plenum	1.6	0.35	300
Steam volume fraction upper plenum	7.7	1.14	45
Steam volume fraction upper annulus	4.9	1.14	45
Helium volume fraction upper plenum	7.7	0.65	300
Helium volume fraction upper annulus	4.6	1.05	305
Helium volume fraction lower plenum	1.7	0.65	60

Table 2. Location of time-dependent measurement transducers.

mixed). During the 2nd phase, a good agreement is observed only for the volume fraction in the upper plenum, whereas during the 3rd phase, the decrease of the simulated steam volume fraction in the upper plenum shows a significant delay. The agreement of helium volume fractions (Figure 13) is good during the 1st phase, when helium was injected. During the 2nd phase, a significant discrepancy may be observed between experimental and simulation results in the upper annulus. In the 3rd phase, a homogenisation of the vessel atmosphere was simulated, while in the experiment the atmosphere remained stratified.

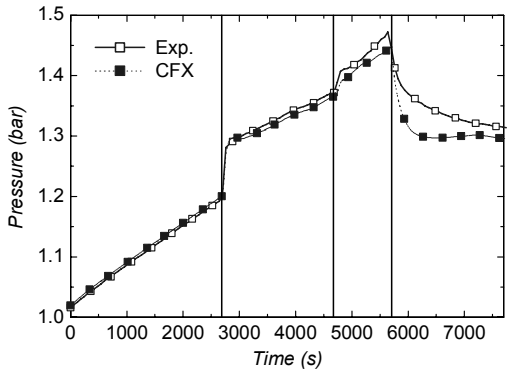

Figure 10. ThAI: measured and calculated pressure.

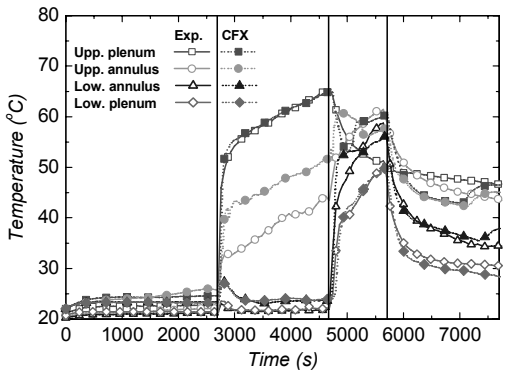

Figure 11. ThAI: measured and calculated atmosphere temperatures.

Figures 14 and 15 show measured and calculated vertical profiles of helium volume fractions at the vessel axis and in the annulus at the ends of the 1st and 2nd phase, whereas figures 16 and 17 show the temperature vertical profiles at the ends of the 2nd and 3rd phase. Despite some discrepancies, the figures reveal that the simulation replicated the compositional and thermal non-homogeneity of the vessel atmosphere reasonably well.

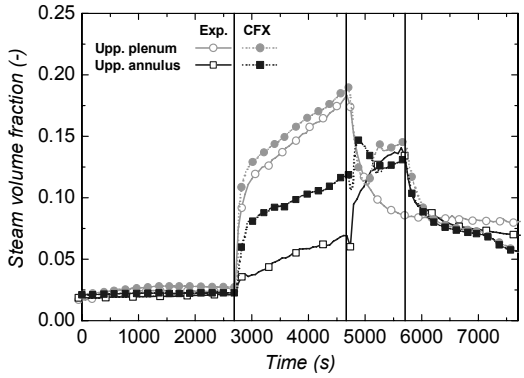

Figure 12. ThAI: measured and calculated steam volume fractions.

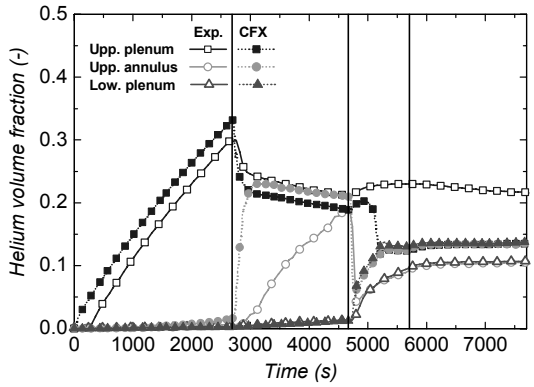

Figure 13. ThAI: measured and calculated helium volume fractions.

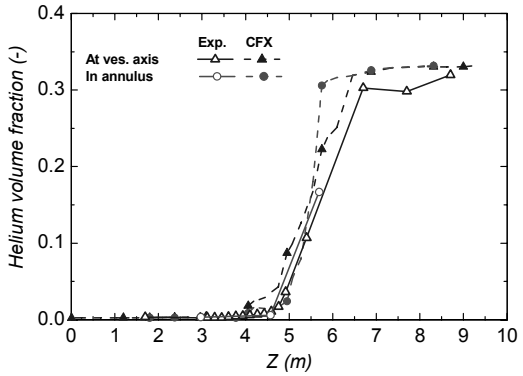

Figure 14. ThAI: measured and calculated helium volume fractions at end of 1st phase (t = 2600 s).

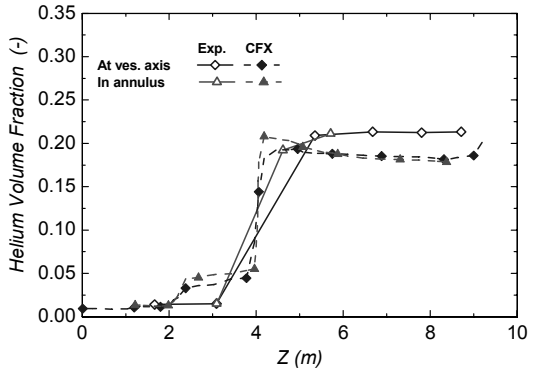

Figure 15. ThAI: measured and calculated helium volume fractions at end of 2nd phase (t = 4600 s).

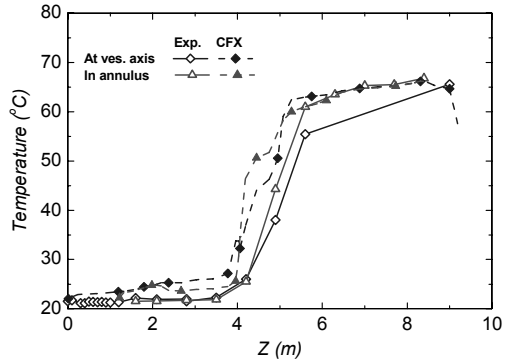

Figure 16. ThAI: measured and calculated atmosphere temperatures at end of 2nd phase (t = 4600 s).

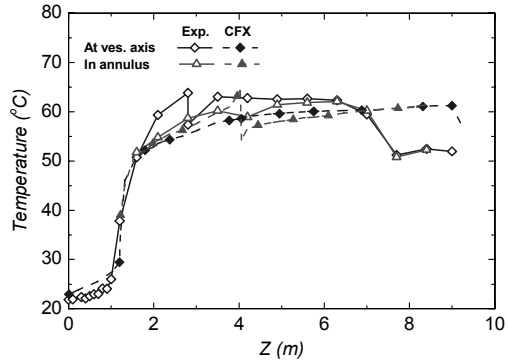

Figure 17. ThAI: measured and calculated atmosphere temperatures at end of 3rd phase (t = 5600 s).

Due to long computation times, rigorous grid-independence tests with grid refinements were not performed.

Conclusions

An approach based on the use of the CFD code CFX was proposed to simulate experiments on containment atmosphere behaviour at accident conditions, which were performed in the TOSQAN and ThAI experimental facilities. The code was complemented with additional models for steam condensation on containment structures and in the containment atmosphere, which were included via user-defined subroutines. Relatively coarse grids were used to allow fast calculations.

The comparison of experimental and calculated results shows that the atmosphere structure was in general well replicated by the simulations, although a tendency to simulate more intensive mixing was observed. Although the proposed method is not totally grid-independent, a good agreement for two different experiments was obtained with similar widths of cells contiguous to condensation surfaces and similar values of the adjustable coefficient in the calculation of the condensation rate. Thus, the proposed approach seems adequate and could in principle be used as a support in the analysis of the safety issue of high local concentration of hydrogen.

Acknowledgments

The presented research was performed within the research project J2-6614 (contract no. 3311-04-8226614) financed by the Ministry of Higher Education, Science and Technology of the Republic of Slovenia.

The Jozef Stefan Institute is a member of the Severe Accident Research Network of Excellence (SARNET) within the 6th EU Framework Programme. The benefit from European Commission RTD Programme for research is acknowledged.

References

[1] Andreani M., Putz F., Dury T., Gjerloev C., Smith B., Application of field codes to the analysis of gas mixing in large volumes, IAEA Tech. Com. Meeting on the Implementation of Hydrogen Mitigation Techniques and Filtered Containment Venting, Koeln, Germany, 2001.

[2] Blumenfeld L. et al., CFD simulation of mixed convection and condensation in a reactor containment / The MICOCO benchmark, Proc.Int. Topical Meeting NURETH-10, Seoul, Korea, 2003.

[3] Martin-Valdepenas J.M., Jimenez M.A., CFD analyses of hydrogen risk within PWR containments, Use of CFD Codes for Safety Analysis of Nuclear Reactor Systems, IAEA-TECDOC-1379, 2003.

[4] Rastogi A.K., CFD application to reactor safety problems with complex flow regimes, Use of CFD Codes for Safety Analysis of Nuclear Reactor Systems, IAEA-TECDOC-1379, 2003.

[5] Siccama N.B., Houkema M., Komen E.M.J., CFD analyses of steam and hydrogen distribution in a nuclear power plant, Use of CFD Codes for Safety Analysis of Nuclear Reactor Systems, IAEA-TECDOC-1379, 2003.

[6] Royl P., Travis J.R., Baumann W., Necker G., Analyses of containment experiments with GASFLOW II, Proc. Int. Topical Meeting NURETH-10, Seoul, Korea, 2003.

[7] Choi Y.S., Lee U.J., Lee J.J., Park G.C., Improvement of HYCA3D code and experimental verification in rectangular geometry, Nuclear Engng Design 226, pp. 337-349, 2003.

[8] Sharma P.K., Markandeya S.G., Ghosh A.K., Kushwaha H.S., Simulation of hydrogen distribution in containment facility – A parametric study using the CFD code FDS, Proc. Int. Conf. ICONE12, Arlington, Virginia, USA, 2004.

[9] Brun Ph. et al., Specification of International Standard Problem on Containment Thermal-Hydraulics ISP-47, Step 1: TOSQAN–MISTRA, IRSN and CEA, Saclay, France, 2002.
[10] Porcheron E. et al., ISP-47 International Standard Problem on Containment Thermal-Hydraulics, Step 1: TOSQAN, Phase B: Air-steam-helium experimental results, IRSN, Saclay, France, 2005.
[11] Caron-Charles M., Quillico J.J., Brinster J., The MISTRA facility for field containment code validation: steam condensation experiments, Proc. Int. Conf. ICONE10, Arlington, USA, 2002.
[12] Fischer K. et al., Containment code comparison exercise on experiment ThAI TH7, Proc. Int. Topical Meeting NURETH-10, Seoul, Korea, 2003.
[13] Fischer K., Specification of the International Standard Problem on Containment Thermal-Hydraulics ISP-47, Step 2: ThAI, Becker Technologies GmbH, Eschborn, Germany, 2004.
[14] Lee U.J., Park G.C., Experimental study on hydrogen behavior at a subcompartment in the containment building, Nuclear Engng Design 217, pp. 41-47, 2002.
[15] AEA Technology plc., CFX-4.4: Solver Manual, Harwell, United Kingdom, 2001.
[16] Porcheron E. et al., International Standard Problem on Containment Thermal-Hydraulics ISP-47, Step 1: TOSQAN–MISTRA, Phase B: Air-steam-helium mixtures, Comparison calculations/ experiment for TOSQAN, IRSN, Saclay, France, 2004.
[17] Fischer K., International Standard Problem ISP-47 on Containment Thermal-Hydraulics, Step 2: ThAI, Vol. 3: Comparison report of open phases I-II followed by blind phases III-IV, Report Nr. BF-R 70031-3, Becker Technologies GmbH, Eschborn, Germany, 2005.
[18] Houkema M., Komen E.M.J., Siccama N.B., Willemsen S.M., CFD analyses of steam and hydrogen distribution in a nuclear power plant, Proc. Int. Topical Meeting NURETH-10, Seoul, Korea, 2003.
[19] Malet J., Porcheron E., Cornet P., Vendel J., Experimental and numerical study of free convective flows with filmwise condensation in a large containment vessel, Proc. 5th Int. Conf. on Multiphase Flow, ICMF'04, Yokohama, Japan, 2004.
[20] Forgione N., Paci S., Computational analysis of vapour condensation in presence of air in the TOSQAN facility, Proc. Int. Topical Meeting NURETH-11, Avignon, France, 2005.
[21] Kljenak I., Babić M., Mavko B., Bajsić I., Modelling of containment atmosphere mixing and stratification experiment using CFD approach, Proc. Int. Topical Meeting NURETH-11, Avignon, France, 2005.
[22] Kljenak I., Babić M., Mavko B., Bajsić I., Modelling of containment atmosphere mixing and stratification experiment using CFD approach, Proc. Int. Conf. ICONE13, Beijing, China, 2005.
[23] Kljenak I., Babić M., Mavko B., Bajsić I., Modelling of containment atmosphere mixing and stratification experiment using CFD approach," submitted to Nuclear Engng Design, 2005.
[24] Babić M., Kljenak I., Mavko B., Simulation of atmosphere mixing and stratification in the ThAI experimental facility with a CFD code, Proc. Int. Conf. "Nuclear Energy for New Europe 2005", Bled, Slovenia, 2005.
[25] Babić M., Kljenak I., Mavko B., Bajsić I., Modeling of non-homogeneous containment atmosphere in the ThAI experimental facility using a CFD code, to be presented at Int. Conf. ICONE14, Miami, Florida, USA, 2005.
[26] Lycklama à Nijeholt J.A., Hart J, CFD simulation of the thermal-hydraulics in the PHEBUS FP containment vessel, Proc. Int. Conf. ICONE-8, Baltimore, USA, 2000.
[27] Smith B.L., Milelli M., Shepel S., Aspects of nuclear reactor simulation requiring the use of advanced CFD models, Use of CFD Codes for Safety Analysis of Nuclear Reactor Systems, IAEA-TECDOC-1379, 2003.
[28] Terasaka H., Makita A., Numerical analysis of the PHEBUS containment thermal-hydraulics, J. Nuclear Science Tech., vol.34, no.7, pp. 666-678, 1996.
[29] Uchida H., Oyama A., Togo Y., Evaluation of post-incident cooling systems of LWR's, Proc. 13th Int. Conf. on Peaceful Uses of Atomic Energy, IAEA, Vienna, Austria, 1965.